Materials Today Physics 34 (2023) 101064

Contents lists available at ScienceDirect

Materials Today Physics

journal homepage: www.journals.elsevier.com/materials-today-physics

# Unraveling the ferroelectric switching mechanisms in ferroelectric pure and La doped $HfO_2$ epitaxial thin films

Alexandre Silva [a,b], Ignasi Fina [c], Florencio Sánchez [c], José P.B. Silva [a,b,**], Luís Marques [a,b], Veniero Lenzi [a,b,*]

[a] Physics Center of Minho and Porto Universities (CF-UM-UP), University of Minho, Campus de Gualtar, 4710-057, Braga, Portugal
[b] Laboratory of Physics for Materials and Emergent Technologies, LapMET, University of Minho, 4710-057, Braga, Portugal
[c] Institut de Ciència de Materials de Barcelona (ICMAB-CSIC), Campus UAB, Bellaterra, 08193, Barcelona, Spain

ARTICLE INFO

*Keywords:*
Ferroelectricity
Epitaxial $HfO_2$ films
Polarization switching
Low-power memory devices

ABSTRACT

Epitaxial orthorhombic phase La doped $HfO_2$ films are promising for achieving robust ferroelectric polarization without wake-up effect. However, lowering the coercive field is crucial for achieving low-power memory devices.

In this work, we have investigated the influence of the La content effect on the structural and ferroelectric properties of epitaxial $HfO_2$ thin films. We show that while the remanent polarization is optimum for 2–5 at. % La-doped $HfO_2$ films, the coercive field is decreased with La doping. The experimental work is supported by density functional theory (DFT) calculations which show that the polarization switching in epitaxial La:$HfO_2$ films can be understood based on the synergetic contribution of the presence of a non-ferroelectric monoclinic phase and the La doping itself that causes a reduction of the nucleation and DW motion energy barriers for the crossing path, which makes it more probable than the non-crossing one.

## 1. Introduction

Ferroelectrics provide promising technical solutions to the desired low-power and high-speed memory for IoT and artificial intelligence (AI) applications [1,2]. In this context, $HfO_2$ and $ZrO_2$-based ferroelectric thin films emerge as the most promising solution, for extensive applications in the non-volatile memory, logic, and neuromorphic devices, due to the CMOS-compatibility and high scalability [3].

Ferroelectricity in $HfO_2$ and $ZrO_2$-based thin films arises from the polar orthorhombic $Pca2_1$ phase (*o*-phase), while in bulk the stable phases are the monoclinic $P2_1/c$ phase (*m*-phase) around room temperature and the tetragonal $P4_2/nmc$ phase (*t*-phase) at high temperature, which are both centrosymmetric showing no ferroelectric behavior [4]. It has been reported that several effects, such as strain, dopants, oxygen vacancies, capping layers, etc, facilitate the *o*-phase formation [5]. However, wake-up effect, imprint, fatigue, and endurance are still drawbacks hindering the commercialization of these devices [6,7]. Better understanding of the properties of ferroelectric $HfO_2$ is needed to solve these drawbacks, and for this objective the use of epitaxial films as model systems can help. In addition, the possibility of growing epitaxial $HfO_2$ and $ZrO_2$-based films appears as a promising solution for eliminating the wake-up effect, while keeping a high endurance and retention [8] [–] [10]. Recently, it was demonstrated that the threshold temperature for the epitaxial growth of $Hf_{0.5}Zr_{0.5}O_2$ (HZO) films is reduced from about 750 °C to about 550 °C by using an ultra-thin HZO seed layer grown at 800 °C [11], which is a remarkable result considering the need to grow epitaxial films at lower temperatures. The films demonstrated encouragingly no wake-up effect, and greatly reduced fatigue and improved endurance.

Another important issue of epitaxial $HfO_2$ and $ZrO_2$-based films is the large coercive field (Ec) that hinders them from realizing low-power memory devices [12]. In this context, the existence of non-ferroelectric phases on epitaxial HZO and $ZrO_2$ films seems to contribute to the decrease of the coercive field [4,13]. Moreover, doping emerges as a promising approach, not only for increasing the ferroelectric polarization, but also for decreasing the coercive field of epitaxial $HfO_2$ and $ZrO_2$-based films. It was recently demonstrated that combined high polarization, high retention, and high endurance is obtained in 2–5 at. % La-doped $HfO_2$ films, while the coercive field is reduced with increasing of La content [14]. However, the physical

* Corresponding author. Physics Center of Minho and Porto Universities (CF-UM-UP), University of Minho, Campus de Gualtar, 4710, Braga, Portugal.
** Corresponding author. Physics Center of Minho and Porto Universities (CF-UM-UP), University of Minho, Campus de Gualtar, 4710-057, Braga, Portugal.
*E-mail addresses:* josesilva@fisica.uminho.pt (J.P.B. Silva), veniero.lenzi@fisica.uminho.pt (V. Lenzi).

https://doi.org/10.1016/j.mtphys.2023.101064
Received 27 February 2023; Received in revised form 24 March 2023; Accepted 27 March 2023
Available online 30 March 2023

mechanism behind the polarization switching dynamics that allows reducing the coercive field in epitaxial $HfO_2$–based films remains to be clarified. Recently, and taking into account that polarization switching is believed to be limited by the intrinsically high energy barrier of ferroelectric domain wall (DW) motions, it was theoretically proposed a new class of topological DWs that allows an unconventional mechanism of ferroelectric polarization switching in o-phase $HfO_2$. Considering the *t*-phase/*o*-phase boundary the energy barriers of DW motion are significantly reduced [15].

As a matter of fact, theoretical studies are currently addressing the polarization switching dynamics in *o*-phase $HfO_2$ [16]. Such systems have recently been shown to possess a rich phase diagram, with previously unaccounted phases that might be playing a role in the switching process [17]. In fact, two competing switching mechanisms [18], with O atoms either crossing or not the Hf planes, which we term here crossing (C) and non-crossing (NC), have been recently identified. This leads to a different assignment of up and down states and thus to a negative or positive piezoelectric coefficient. Further, it was recently proposed that the DW motion occurs through the crossing path implying, among other things, that the maximal FE polarization value should be 70 $\mu C/cm^2$, larger than the currently accepted value [19].

While the polarization switching dynamics in *o*-phase $HfO_2$ has been studied in detail [20], including the effects of strain [21], the role of the boundary between the *o*-phase and the *m*-phase on the polarization switching and its impact on the coercive field was not investigated in detail. In addition, while it is known that doping affects the switching barriers [22,23] and it was experimentally observed that La doping reduces the coercive field [14], the physical mechanism responsible for this observation needs to be further investigated.

Therefore, in this work, we first provide experimental evidence for the role of La doping content on the structural and ferroelectric properties of La:$HfO_2$ films. Next, using density functional theory (DFT) calculations, we assess the distinct influences of the presence of non-ferroelectric m-phase in $HfO_2$ films and then the La content impact on the polarization switching of La:$HfO_2$ epitaxial films.

## 2. Materials and methods

La:$HfO_2$ films (2 and 5 at% La content) of thickness about 8.5 nm were grown on $La_{0.67}Sr_{0.33}MnO_3$ (LSMO) buffered (001)-oriented $SrTiO_3$ (STO) substrates by pulsed laser deposition using a KrF excimer laser. Platinum circular top electrodes (diameter 20 μm and thickness 20 nm) were grown ex-situ at room temperature by magnetron sputtering through stencil masks. X-ray diffraction (XRD) characterization was done with Cu Kα radiation using a Bruker D8-Advance diffractometer equipped with a 2D detector. Ferroelectric characterization was done using an AixACCT TFAnalyser2000 platform. Polarization loops were measured at 1 kHz by the Positive-Up Negative-Down (PUND) procedure at room temperature in top-bottom configuration, with the bottom LSMO electrode grounded. Additional experimental conditions are reported elsewhere [14,24].

All DFT calculations have been performed using VASP [25] [–] [27], employing the PBEsol [28] functional and a cutoff energy of 600 eV was chosen for all calculations. A 6 × 1 × 1 supercell containing *o*-phase and/or *m*-phase unit cells was constructed, and a Γ-centered 1 × 3 × 3 k-point grid was considered. Structural relaxations for initial and final structures were carried on until forces converged to a threshold of 10 meV/Å. For La doped systems, spin polarized calculations were performed. The polarization switching energy barriers have been calculated using the generalized solid state nudged elastic band (NEB) method [29], as implemented in the VTST routines of Henkel group [30], with a force convergence threshold of 30 meV/Å, a convergence threshold for the stress tensor components of 0.1 GPa and using a minimum of 8 images per pathway. Atomic structure representations were obtained using VESTA [31].

## 3. Results

### 3.1. Experimental characterization of La doped $HfO_2$ epitaxial thin films

Fig. 1 shows XRD 2θ-χ maps of 2 at% La doped (a) and 5 at% La doped (b) $HfO_2$ films, with 2θ scans integrated from $\chi = -10^\circ$ to $\chi = +10^\circ$ in the corresponding bottom panels. All samples exhibit a bright spot at 2θ ~30°, which is the position of the orthorhombic (o) (111), tetragonal (101), and cubic (111) reflections. In addition, the monoclinic (−111) reflection is visible in the 2 at% La film and it is not present in the 5 at% La film. The current-voltage and polarization-voltage loops are shown in Fig. 1(c) and (d), respectively. The ferroelectric switching peaks are well visible in the 2% and 5% films, exhibiting high remanent polarization of about 22 and 18 $\mu C/cm^2$, respectively. The ferroelectric polarization values, together with dielectric permittivity (see data in Ref. [14]), indicates that 2 at% La film has the greatest orthorhombic phase content. With increasing La content paraelectric cubic phase is favored lowering polarization in the 5 at% La film and null polarization in the 10 at % La film [14]. The coercive electric field reduces with increasing La content, being about 4.1 and 3.3 V in the 2 and 5 at% La, respectively. The current versus voltage for twin 2 and 5% La:$HfO_2$ samples is shown in Fig. S1 [14]. It can be observed that leakage current density is around $1.5 \times 10^{-7}$ and $1 \times 10^{-6}$ $A/cm^2$ at 1 and 2 V for both samples. The leakage is comparable to that of other epitaxial films of doped $HfO_2$ of similar thickness [32].

### 3.2. Density functional theory calculations of nucleation and domain wall motion energies

NEB calculations were performed to elucidate the role of parasitic secondary phases, such as the *m*-phase, and the La doping effect in *o*-phase $HfO_2$ films. For simplicity, we investigated first the switching mechanisms in pure $HfO_2$ and then the role of La doping on the switching mechanisms.

#### 3.2.1. Role of secondary phases on the ferroelectric switching of $HfO_2$

The FE polarization switching mechanism in *o*-phase $HfO_2$ is illustrated in Fig. 2(a). It occurs via the displacement along the c direction of the two symmetry equivalent O1 oxygen atoms, which could either cross or not the Hf atom plane (see Fig. 2(a)), hence making for the two different crossing and non-crossing paths [18]. By employing a pure *o*-phase 6 × 1 × 1 supercell, it is possible to calculate the nucleation energy, understood as the energy to switch one domain in a uniformly polarized system, and the domain wall motion energy (see Fig. 2(b)).

For the NC switching mechanism (black line in Fig. 2(c)) a nucleation energy of 1.33 eV was found, and a DW motion energy of 0.86 eV. For the C switching mechanism (red line in Fig. 2(c)), a nucleation energy of 0.86 eV and a DW motion energy of 0.36 eV were found. Those results are in agreement with previously reported calculations [15,19]. Regarding the DW motion, the mechanism occurs through an intermediate non-polar phase that could be identified as a monoclinic phase.

Concerning *o*-/*m*-interfaces, we decided to investigate the o(010)/m (100) interface, since it has been identified in $HfO_2$ films and was suggested to be highly mobile [33]. A 6 × 1 × 1 supercell composed by 3 *o*-phase with aligned polarization and 3 *m*-phase cells has been constructed, as represented in Fig. 3(a) and the polarization energies have been calculated for both the crossing and non-crossing cases. In particular, given the initial supercell, there are 4 inequivalent switching sites, represented in Fig. 3(b): *o*-phase domains, either at the interface (N1) or not (N3); or *m*-phase domains, either at the interface (N2) or not (N4).

Fig. 4 reports the nudged elastic band (NEB) results for the switching energy barriers for the cases shown in Fig. 3(b). Compared to the pure *o*-phase (black lines), the presence of the interface with the *m*-phase lowers the barriers in all the sites and switching paths considered. It is interesting to observe that, while the switching at sites N2 and N4 is a 2-state process (for both C and NC paths) the switching at sites N1 (both C

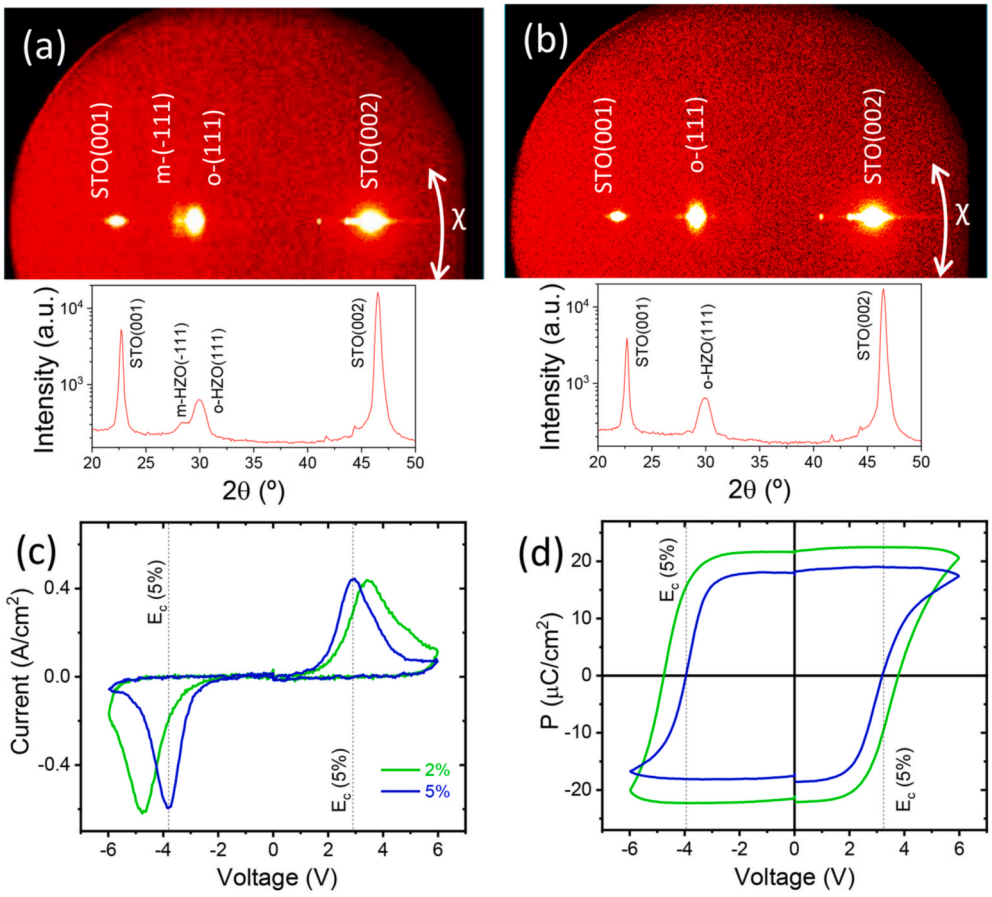


**Fig. 1.** XRD 2θ-χ maps of 2 at% La doped (a) and 5 at% La doped (b) $HfO_2$ films, with 2θ scans integrated around $\chi = 0°$. Current-voltage (c) and polarization - voltage (d) loops of the of 2 at% La doped (green line) and 5 at% La doped (blue line) $HfO_2$ films. (For interpretation of the references to color in this figure legend, the reader is referred to the Web version of this article.)

and NC) and N3 (NC only) appears to be a 3-state process. Upon closer inspection, we found that the intermediate lowest-energy state could be identified as *m*-phase, indicating that there is a u-> m-> d switching path. This means that there is a possibility for the switching domain to be trapped into the *m*-phase state, losing its polarization.

Therefore, our calculations suggest that the presence of the *m*-phase in *o*-phase $HfO_2$ films reduces the polarization switching energy barriers, and so, at the interface, the nucleation process costs less energy and thus is more easily initiated than in pure *o*-phase bulk. Furthermore, interfaces with *t*-phase can also provide a reduction in Ec, as demonstrated theoretically [15].

### 3.2.2. *La doping effect on the ferroelectric switching of $HfO_2$ films*

To study the effect of La doping on the domain switching barriers of *o*-phase $HfO_2$ films, we considered a single La substitution in a $6 \times 1 \times 1$ *o*-phase supercell, corresponding to a doping level of 4 Hf at %. In the *o*-phase, the La substitution induces a distortion of the polar domain of the *o*-phase, as shown in Fig. 5(a). We calculated switching energy barriers of the *o*-phase domain that includes the La atom considering both a nucleation (Fig. 5(b)) and a domain wall movement (Fig. 5(c)).

Concerning nucleation barriers (Fig. 5(b)), we observe a 13% larger energy barrier for the NC path and a 80% lower one for the crossing path. While the NC path is only slightly affected by La: doping, the C path is greatly reduced, suggesting that La doped sites provide favorable nucleation sites.

A similar, but less pronounced, effect is found for the DW motion energy barriers (Fig. 5(c)): the non-crossing pathway shows a slightly increased maximum when compared with the undoped case, from 0.8 eV to 1.1 eV. Conversely, we observe for the crossing pathway a slight decrease in switching energy, from 0.4 eV to 0.25 eV. Thus, the La presence greatly enhances the C path over the NC one. This is clearly aligned with the experimental observations (see Fig. 1) that shows that the increase in the La content from 2% up to 5% decreases the Ec value. It is interesting to note that, in both cases, the *m*-phase intermediate formation is suppressed by the presence of La, resulting in a 2-step switching process. This prevents the polar domain from being trapped into a lower and non-FE energy state.

The effect of La presence at the interface has also been characterized at the *o/m* interface, by calculating the domain switching energy for the N1 switching site (Fig. 3(b)) in presence of a La atom at the *o/m* interface. The results are reported in Fig. 6, for both C and NC paths. As observed for the domain switching in the pure *o*-phase (Fig. 5(c)), La atoms located at the *o/m* interface suppress the formation of the intermediate *m*-like state for both paths, and enhance the energy difference in the paths, that is by lowering the C-path barrier and raising the NC path barrier.

From the DFT calculations (sections 3.2.1 and 3.2.2) we can conclude that the presence of a non-ferroelectric *m*-phase and the La doping causes the decrease of the Ec value. However, in section 3.1 it is observed that La doping also causes the suppression of the parasitic *m*-phase in the La:$HfO_2$ films, which seems to contradict the DFT calculations from the previous section. Indeed, the effect of the La content increase appears superimposed on the effect of the existence of the parasitic *m*-phase, which leads to a decrease in the Ec value. Given the reduction of the switching barriers for the C path caused by the doping effect, the La doping seems to be the dominant effect. Nevertheless, both effects should be considered towards lowering the Ec value of memory devices.

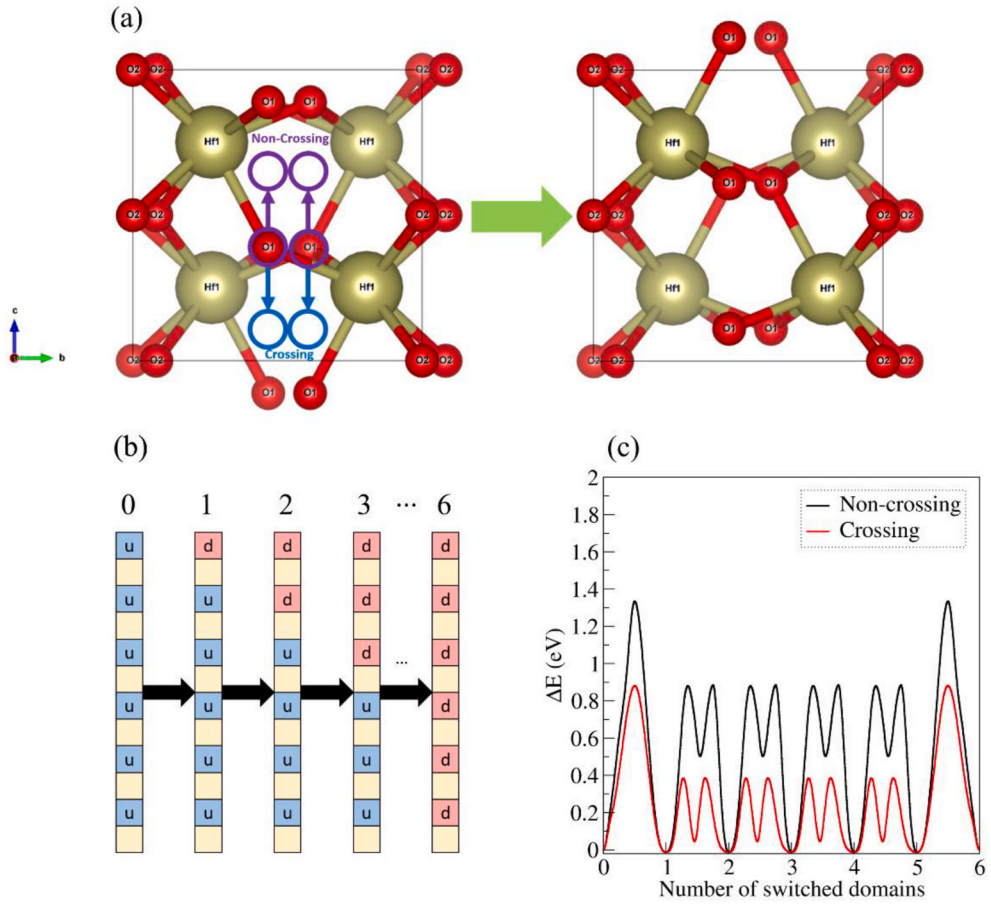


**Fig. 2.** (a) Representation of the two possible polarization switching paths in a *o*-phase $HfO_2$ unit cell. The O atoms labeled O1 displace along *c* axis, either crossing or not the Hf plane. Here and in the remainder, O atoms are red and Hf atoms are ochre. (b) Schematic representation of the switching of a 6 × 1 × 1 cell, from up-polarized (u) to down polarized (d), through the motion of the domain wall between the differently-polarized phases. The numbers indicate the sequence in which domains are switched. (c) NEB calculation results for the mechanism represented in panel (b), for crossing and non-crossing paths. (For interpretation of the references to color in this figure legend, the reader is referred to the Web version of this article.)

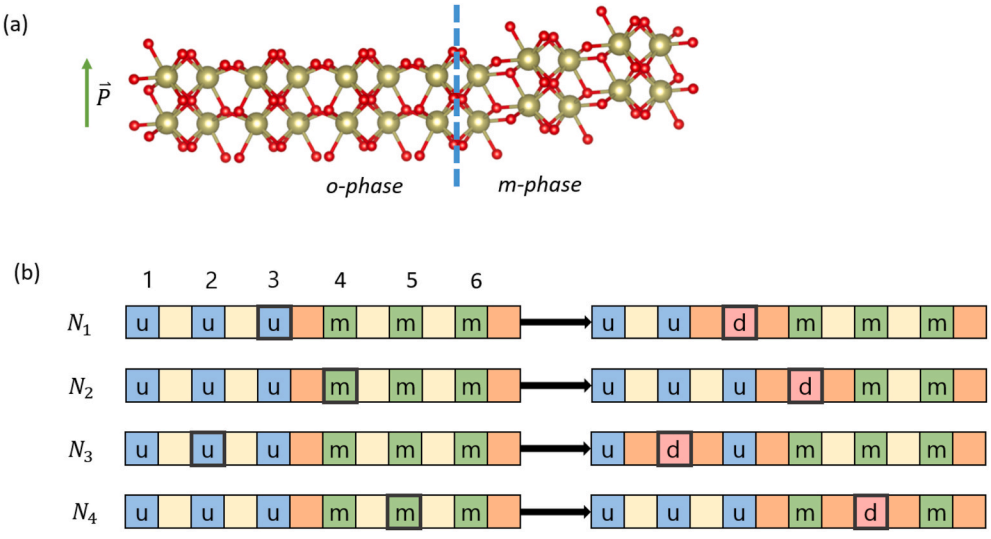


**Fig. 3.** Representation of the 6 × 1 × 1 supercell cell realizing the o-(010)-m(001) interface, comprised by 3 *o*-phase unit cells and 3 *m*-phase ones. The green arrow indicates the direction of spontaneous polarization in the *o*-phase and the dashed lines indicates the *o*/*m* interface. (b) Diagram illustrating the possible switching sites in the interface supercell. u and d indicate up- and down polarized *o*-phase domains, respectively, m stands for *m*-phase domains and non-polar tetragonal-like spacers are represented by unmarked squares. Orange-colored squares denote domain walls between o-phase domains with different polarization or between *o*-phase and *m*-phase. (For interpretation of the references to color in this figure legend, the reader is referred to the Web version of this article.)

## 4. Conclusions

The effects of the presence of a non-ferroelectric *m*-phase and the La doping on the coercive field of $HfO_2$ thin films has been investigated experimentally and theoretically to explain the reduction of Ec observed in ferroelectric epitaxial La:$HfO_2$ thin films. Both effects cause the lowering of the switching energy barriers *per se*, which can be reflected in the reduction of Ec value. However, in La:$HfO_2$ films the increase of the La content suppresses the formation of the *m*-phase, leading to its disappearance at 5% doping concentration.

First, it was demonstrated that the presence of *m*-phase is beneficial in terms of Ec reduction. At the *o*/*m* interface, the polarization switching barriers are lower for all the possible switching sites and paths, when compared to the pure *o*-phase nucleation. Further, it was found that the La presence dramatically decreases the nucleation and DW motion energy barriers for the C energy path. This has a two-fold effect on the polarization switching dynamics of the film: not only the DW energy decrease reduces Ec, as observed experimentally, but also each La site

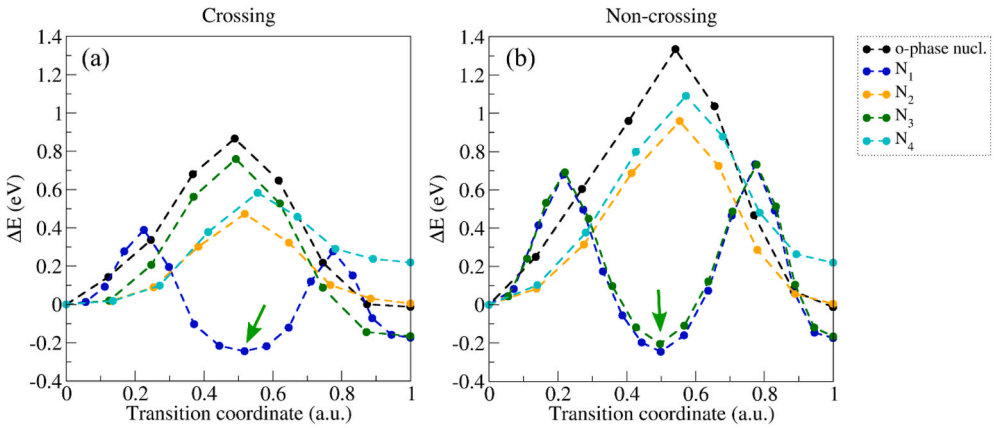


**Fig. 4.** Polarization switching energy barriers calculated for the cases of Fig. 2(b), for the C(a) and NC(b) paths. Black lines represent the nucleation in a pure *o*-phase $6 \times 1 \times 1$ supercell. The green arrows indicate the *m*-phase intermediate state. Lines are a guide for the eye. (For interpretation of the references to color in this figure legend, the reader is referred to the Web version of this article.)

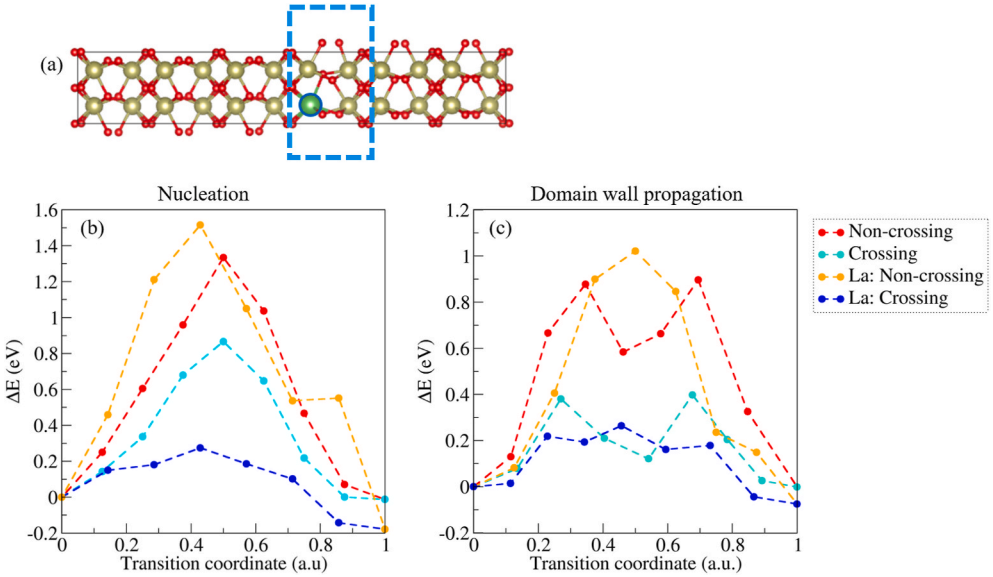


**Fig. 5.** (a) Representation of the o/o interface in a La (green atom) doped $6 \times 1 \times 1$ $HfO_2$ supercell. The distorted domain considered for switching barrier calculation is highlighted by the blue dashed rectangle. (b) Comparison between La doped and undoped switching energy barriers for the crossing and non-crossing paths of a nucleation process (c) Comparison between La doped and undoped switching energy barriers for the crossing and non-crossing paths of a domain wall motion process. Lines are a guide for the eye. (For interpretation of the references to color in this figure legend, the reader is referred to the Web version of this article.)

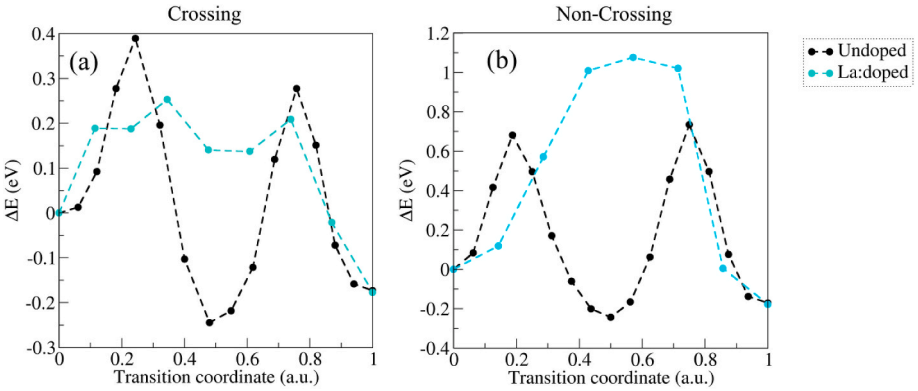


**Fig. 6.** NEB calculation results for the crossing (a) and non-crossing (b) switching paths at the *o*/*m* interface, with and without La doping, for the $N_1$ process of Fig. 3. Lines are a guide for the eye.

provides a favorable nucleation site for switching. Finally, it was found that when La atoms are present at the *o*/*m* interface, it suppresses the formation of the intermediate *m*-phase like domains in the *o*-phase switching process.

We believe that similar studies on $HfO_2$ and $ZrO_2$-based films with different dopants and considering other paraelectric phases, such as the cubic phase, will follow with the aim of achieving low-power ferroelectric memory devices.

## Credit author statement

**A.S.**: Investigation; Methodology; Writing – original draft. **I.F.**: Funding acquisition; Investigation; Methodology; Resources; Writing – review and editing. **F.S.**: Funding acquisition; Investigation; Methodology; Resources; Writing – review and editing. **J.P.B.S.**: Funding acquisition; Investigation; Methodology; Resources; Writing – review and editing. **L.M.**: Funding acquisition; Resources; Supervision; Writing – review and editing. **V.L.**: Conceptualization; Supervision; Writing –review and editing.

## Declaration of competing interest

The authors declare that they have no known competing financial interests or personal relationships that could have appeared to influence the work reported in this paper.

## Data availability

Data will be made available on request.

## Acknowledgements

Financial support from the Spanish Ministry of Science and Innovation (MCIN/AEI/10.13039/501100011033), through the Severo Ochoa FUNFUTURE (CEX2019-000917-S), PID2020-112548RB-I00 and PID2019-107727RB-I00 projects, and from Generalitat de Catalunya (2021 SGR 00804) is acknowledged. We also acknowledge project TED2021-130453B–C21, funded by MCIN/AEI/10.13039/501100011033 and European Union NextGeneration EU/PRTR. This work was supported by: (i) the Portuguese Foundation for Science and Technology (FCT) in the framework of the Strategic Funding Contract UIDB/04650/2020; (ii) exploratory project 2022.01740.PDTC and (iii) the European Union's Horizon 2020 research and innovation programme under grant agreement No 958174 (M-ERA-NET3/0003/2021 - NanOx4EStor). J. P. B. S. also thanks FCT for the contract under the Institutional Call to Scientific Employment Stimulus – 2021 Call (CEECINST/00018/2021). A.S. also acknowledges FCT for the PhD grant with reference 2022.13796.BD.

## Appendix A. Supplementary data

Supplementary data to this article can be found online at https://doi.org/10.1016/j.mtphys.2023.101064.

## References

[1] M. Kobayashi, J. Wu, Y. Sawabe, S. Takuya, T. Hiramoto, Mesoscopic-scale grain formation in $HfO_2$-based ferroelectric thin films and its impact on electrical characteristics, Nano Convergence 9 (2022) 50, https://doi.org/10.1186/s40580-022-00342-6.

[2] B. Cui, Z. Fan, W. Li, Y. Chen, S. Dong, Z. Tan, S. Cheng, B. Tian, R. Tao, G. Tian, D. Chen, Z. Hou, M. Qin, M. Zeng, X. Lu, G. Zhou, X. Gao, J.-M. Liu, Ferroelectric photosensor network: an advanced hardware solution to real-time machine vision, Nat. Commun. 13 (2022) 1707, https://doi.org/10.1038/s41467-022-29364-8.

[3] U. Schroeder, M.H. Park, T. Mikolajick, C.S. Hwang, The fundamentals and applications of ferroelectric $HfO_2$, Nat. Rev. Mater. 7 (2022) 653–669, https://doi.org/10.1038/s41578-022-00431-2.

[4] J.P.B. Silva, K.C. Sekhar, R.F. Negrea, J.L. MacManus-Driscoll, L. Pintilie, Progress and perspective on different strategies to achieve wake-up-free ferroelectric hafnia and zirconia-based thin films, Appl. Mater. Today 26 (2022): 101394, https://doi.org/10.1016/j.apmt.2022.101394.

[5] A.P.S. Crema, M.C. Istrate, A. Silva, V. Lenzi, L. Domingues, M.O. Hill, V. S. Teodorescu, C. Ghica, M.J.M. Gomes, M. Pereira, L. Marques, J.L. MacManus-Driscoll, J.P.B. Silva, Ferroelectric Orthorhombic ZrO2 Thin Films Achieved Through Nanosecond Laser Annealing, Adv. Sci. (2023) 2207390, https://doi.org/10.1002/advs.202207390.

[6] J. Bouaziz, P.R. Romeo, N. Baboux, B. Vilquin, Huge reduction of the wake-up effect in ferroelectric HZO thin films, ACS Appl. Electron. Mater. 1 (2019) 1740–1745, https://doi.org/10.1021/acsaelm.9b00367.

[7] V. Lenzi, J.P.B. Silva, B. Šmíd, V. Matolín, C.M. Istrate, C. Ghica, J.L. MacManus-Driscoll, L. Marques, Ferroelectricity induced by oxygen vacancies in rhombohedral $ZrO_2$ thin films, Energy Environ. Mater. (2022): e12500, https://doi.org/10.1002/eem2.12500.

[8] I. Fina, F. Sánchez, Epitaxial ferroelectric $HfO_2$ films: growth, properties, and devices, ACS Appl. Electron. Mater. 3 (2021) 1530–1549, https://doi.org/10.1021/acsaelm.1c00110.

[9] J.P.B. Silva, M.C. Istrate, M. Hellenbrand, A. Jan, M.T. Becker, J. Symonowicz, F. G. Figueiras, V. Lenzi, M.O. Hill, C. Ghica, K.N. Romanyuk, M.J.M. Gomes, G. D. Martino, L. Marques, J.L. MacManus-Driscoll, Ferroelectricity and negative piezoelectric coefficient in orthorhombic phase pure $ZrO_2$ thin films, Appl. Mater. Today 30 (2023): 101708, https://doi.org/10.1016/j.apmt.2022.101708.

[10] Y. Luo, Z. Tang, X. Yin, C. Chen, Z. Fan, M. Qin, M. Zeng, G. Zhou, X. Gao, X. Lu, J. Dai, D. Chen, J.-M. Liu, Ferroelectricity in dopant-free $HfO_2$ thin films prepared by pulsed laser deposition, J. Mater. 8 (2022) 311–318, https://doi.org/10.1016/j.jmat.2021.09.005.

[11] T. Song, R. Bachelet, G. Saint-Girons, I. Fina, F. Sanchez, Ferroelectric $Hf_{0.5}Zr_{0.5}O_2$ films with improved endurance obtained through low temperature epitaxial growth on seed layers, Nanoscale (2023), https://doi.org/10.1039/D2NR05935E.

[12] B. Noheda, J. Íñiguez, A key piece of the ferroelectric hafnia puzzle, Science 369 (2020) 1300–1301, https://doi.org/10.1126/science.abd1212.

[13] T. Song, F. Sánchez, I. Fina, Impact of non-ferroelectric phases on switching dynamics in epitaxial ferroelectric $Hf_{0.5}Zr_{0.5}O_2$ films, APL Mater. 10 (2022): 031108, https://doi.org/10.1063/5.0083661.

[14] T. Song, H. Tan, R. Bachelet, G. Saint-Girons, I. Fina, F. Sánchez, Impact of La concentration on ferroelectricity of La-doped $HfO_2$ epitaxial thin films, ACS Appl. Electron. Mater. 3 (2021) 4809–4816, https://doi.org/10.1021/acsaelm.1c00672.

[15] D.-H. Choe, S. Kim, T. Moon, S. Jo, H. Bae, S.-G. Nam, Y.S. Lee, J. Heo, Unexpectedly low barrier of ferroelectric switching in $HfO_2$ via topological domain walls, Mater. Today 50 (2021) 8–15, https://doi.org/10.1016/j.mattod.2021.07.022.

[16] D.H. Lee, Y. Lee, K. Yang, J.Y. Park, S.H. Kim, P.R.S. Reddy, M. Materano, H. Mulaosmanovic, T. Mikolajick, J.L. Jones, U. Schroeder, M.H. Park, Domains and domain dynamics in fluorite-structured ferroelectrics, Appl. Phys. Rev. 8 (2021): 021312, https://doi.org/10.1063/5.0047977.

[17] A. Kersch, M. Falkowski, New low-energy crystal structures in $ZrO_2$ and $HfO_2$, Phys. Status Solidi Rapid Res. Lett. 15 (2021): 2100074, https://doi.org/10.1002/pssr.202100074.

[18] Y. Qi, S.E. Reyes-Lillo, K.M. Rabe, "Double-path" Ferroelectrics and the Sign of the Piezoelectric Response, 2022, https://doi.org/10.48550/arXiv.2204.06999.

[19] Y. Wu, Y. Zhang, J. Jiang, L. Jiang, M. Tang, Y. Zhou, E.Y. Tsymbal, M. Liao, Q. Yang, Polarization Switching Mechanism of (Hf, Zr)$O_2$ Ferroelectrics Driven by Domain Wall Motion, 2023, https://doi.org/10.48550/arXiv.2301.06248.

[20] W. Ding, Y. Zhang, L. Tao, Q. Yang, Y. Zhou, The atomic-scale domain wall structure and motion in $HfO_2$-based ferroelectrics: a first-principle study, Acta Mater. 196 (2020) 556–564, https://doi.org/10.1016/j.actamat.2020.07.012.

[21] W. Wei, G. Zhao, X. Zhan, W. Zhang, P. Sang, Q. Wang, L. Tai, Q. Luo, Y. Li, C. Li, J. Chen, Switching pathway-dependent strain-effects on the ferroelectric properties and structural deformations in orthorhombic $HfO_2$, J. Appl. Phys. 131 (2022): 154101, https://doi.org/10.1063/5.0084660.

[22] K. Chae, A.C. Kummel, K. Cho, Tetravalent doping in fluorite-based ferroelectric oxides for reduced voltage operations, ACS Appl. Mater. Interfaces 14 (2022) 29007–29013, https://doi.org/10.1021/acsami.2c05886.

[23] H. Yang, H.-J. Lee, J. Jo, C.H. Kim, J.H. Lee, Role of Si doping in reducing coercive field for ferroelectric switching in $HfO_2$, Phys. Rev. Applied 14 (2020): 064012, https://doi.org/10.1103/PhysRevApplied.14.064012.

[24] T. Song, S. Estandía, I. Fina, F. Sánchez, Ferroelectric (Hf,Zr,La)$O_2$ films, Appl. Mater. Today 29 (2022): 101661, https://doi.org/10.1016/j.apmt.2022.101661.

[25] G. Kresse, J. Hafner, *Ab initio* molecular dynamics for liquid metals, Phys. Rev. B 47 (1993) 558–561, https://doi.org/10.1103/PhysRevB.47.558.

[26] G. Kresse, J. Furthmüller, Efficient iterative schemes for *ab initio* total-energy calculations using a plane-wave basis set, Phys. Rev. B 54 (1996) 11169–11186, https://doi.org/10.1103/PhysRevB.54.11169.

[27] G. Kresse, J. Furthmüller, Efficiency of ab-initio total energy calculations for metals and semiconductors using a plane-wave basis set, Comput. Mater. Sci. 6 (1996) 15–50, https://doi.org/10.1016/0927-0256(96)00008-0.

[28] J.P. Perdew, A. Ruzsinszky, G.I. Csonka, O.A. Vydrov, G.E. Scuseria, L. A. Constantin, X. Zhou, K. Burke, Restoring the density-gradient expansion for exchange in solids and surfaces, Phys. Rev. Lett. 100 (2008): 136406, https://doi.org/10.1103/PhysRevLett.100.136406.

[29] D. Sheppard, P. Xiao, W. Chemelewski, D.D. Johnson, G. Henkelman, A generalized solid-state nudged elastic band method, J. Chem. Phys. 136 (2012): 074103, https://doi.org/10.1063/1.3684549.

[30] Transition state tools for VASP — transition state tools for VASP. https://theory.cm.utexas.edu/vtsttools/. (Accessed 18 February 2023) accessed.

[31] K. Momma, F. Izumi, *VESTA 3* for three-dimensional visualization of crystal, volumetric and morphology data, J. Appl. Crystallogr. 44 (2011) 1272–1276, https://doi.org/10.1107/S0021889811038970.

[32] T. Song, R. Bachelet, G. Saint-Girons, R. Solanas, I. Fina, F. Sánchez, Epitaxial ferroelectric La-doped $Hf_{0.5}Zr_{0.5}O_2$ thin films, ACS Appl. Electron. Mater. 2 (2020) 3221–3232, https://doi.org/10.1021/acsaelm.0c00560.

[33] E.D. Grimley, T. Schenk, T. Mikolajick, U. Schroeder, J.M. LeBeau, Atomic structure of domain and interphase boundaries in ferroelectric $HfO_2$, Adv. Mater. Interfac. 5 (2018): 1701258, https://doi.org/10.1002/admi.201701258.